International Journal of Pharmaceutics 358 (2008) 238–247

Contents lists available at ScienceDirect

International Journal of Pharmaceutics

journal homepage: www.elsevier.com/locate/ijpharm

Experimental observations of dry powder inhaler dose fluidisation

Rob Tuley[a], John Shrimpton[a,*], Matthew D. Jones[b], Rob Price[b], Mark Palmer[c], Dave Prime[c]

[a] Mechanical Engineering Department, Imperial College London SW7 2AZ, UK
[b] Pharmaceutical Surface Science Research Group, Department of Pharmacy & Pharmacology, University of Bath, UK
[c] Inhalation Product Development, GSK R&D, Ware, UK

ARTICLE INFO

Article history:
Received 17 October 2007
Received in revised form 10 March 2008
Accepted 13 March 2008
Available online 1 April 2008

Keywords:
Dry powder inhaler
Fluidisation
Lactose
Powder flow
Inhalation
Shear cello

ABSTRACT

Dry powder inhalers (DPIs) are widely used to deliver respiratory medication as a fine powder. This study investigates the physical mechanism of DPI operation, assessing the effects of geometry, inhalation and powder type on dose fluidisation. Patient inhalation through an idealised DPI was simulated as a linearly increasing pressure drop across three powder dose reservoir geometries permitting an analysis of shear and normal forces on dose evacuation. Pressure drop gradients of 3.3, 10 and 30 kPa s^{-1} were applied to four powder types (glass, aluminium, and lactose 6 and 16% fines) and high speed video of each powder dose fluidisation was recorded and quantitatively analysed. Two distinct mechanisms are identified, labelled 'fracture' and 'erosion'. 'Fracture' mode occurs when the initial evacuation occurs in several large agglomerates whilst 'erosion' mode occurs gradually, with successive layers being evacuated by the high speed gas flow at the bed/gas interface. The mechanism depends on the powder type, and is independent of the reservoir geometries or pressure drop gradients tested. Both lactose powders exhibit fracture characteristics, while aluminium and glass powders fluidise as an erosion. Further analysis of the four powder types by an annular shear cell showed that the fluidisation mechanism cannot be predicted using bulk powder properties.

1. Introduction

The dry powder inhaler (DPI) has in recent years become a common method of asthma treatment. In these devices a dose of fine particles is fluidised by exposure to a stream of air inhaled by the patient. The growing interest in using DPIs to deliver therapeutic proteins and peptides (e.g. insulin) (Shoyele and Slowey, 2006), and the increasing popularity of the technology among patient groups as an asthma treatment (Borgstrom et al., 2002) indicates that DPIs have an important future in respiratory drug delivery. However, at present there are few reported experimental studies that examine the dynamics of the particle population *within* a DPI during its operation. An understanding of this initial stage of powder evacuation from the DPI is of critical importance in the prediction of the powder agglomeration and velocity at the exit of the inhaler, which defines device performance.

The physics governing the powder dose fluidisation within a DPI are very complex but a number of parallels can be drawn with other areas of research, specifically fluidised bed technology and pneumatic conveying. In a fluidised bed, air is blown vertically upwards through a packed powder bed. The upward force of the flow on the particles counterbalances their weight, and the powder bed becomes 'fluidised' in that it flows like a liquid. Pneumatic conveying applies this principle to horizontal flows: powder can be transported along a channel by using a flow that helps to push it in the right direction. The process that occurs within a DPI is related to both fields: the powder dose is pneumatically conveyed out of the inhaler by an airflow, and the solid powder bed is usually fluidised to achieve this.

Research into fluidised bed technology and pneumatic conveying is extensive (Sundaresan, 2003; Molerus, 1996), and for both fields a number of distinct behaviours have been identified. In each case the dominate factor in determining the regime is the material properties of the powder itself (Sanchez et al., 2003; Geldart, 1973). The common problem is in adequately characterising a powder using its material properties to predict its behaviour. The properties relevant to particle/air interaction include those such as particle size distribution, density, shape and surface characteristics. However, traditional methods of particle characterisation (such as shear testing) measure steady state *bulk* properties, that do not adequately define these parameters.

For fluidised bed technology, Geldart classified powders into four categories (A, B, C and D) based on the volumetric mean particle diameter, d_p, and the difference between particle solid density ρ_s and gas density ρ_g (Geldart, 1973). Each category exhibits different trends in fluidisation behaviour. Although this grouping is an

* Corresponding author. Tel.: +44 2075947157.
E-mail address: j.shrimpton@imperial.ac.ukz (J. Shrimpton).

0378-5173/$ – see front matter © 2008 Elsevier B.V. All rights reserved.
doi:10.1016/j.ijpharm.2008.03.038

Nomenclature

d_p	mean particle diameter
DPI	dry powder inhaler
ff_c	flowability
FPF	fine particle fraction
FPS	frames per second
RH	relative humidity

Greek letters

ε	porosity
ρ_b	bulk density
ρ_g	gas density
ρ_s	solid density
σ_c	unconfined yield strength
σ_{pre}	pre-shearing stress
τ_0	cohesion

empirical correlation based on a limited set of powder properties, it is still widely used to predict powder fluidisation characteristics. Dixon (1979) used Geldart's work to create a similar four group classification for pneumatic conveyance.

The field of DPI characterisation is less mature than either fluidised bed technology or pneumatic conveyance, and the majority of studies to date focus on either powder formulation or performance characterisation of specific devices for regulatory approval (Chan, 2006). The powder formulation used for asthma treatment commonly consists of a blend of coarse lactose 'carrier' particles and fine active drug. The performance of a particular powder blend in a DPI can be quantified using radionuclide imaging techniques to measure the active drug deposition in the lungs (Newman and Pitcairn, 2005). Good performance is usually associated with a high fine particle fraction (FPF, the mass fraction of individual or agglomerated particles less than approximately 5 μm in the aerosol) exiting the inhaler, as smaller particles are more likely to reach the lungs upon inhalation (Clark and Borgstrom, 2002). Techniques such as Cascade–Impactor experiments (Dunbar and Hickey, 2000) are used to evaluate the FPF emerging from a DPI under the influence of patient inhalation. This FPF is known to be strongly affected by factors such as the powder formulation size distribution, cohesivity and other material properties in addition to external factors such as ambient humidity (Chew and Chan, 2002). In such experiments the measured FPF is obtained downstream of the DPI exit, and thus does not provide any insight into the actual operation of the device, or the mechanisms of powder bed break-up that occur within it.

It is generally acknowledged that the design of the DPI does have a significant effect on the FPF (Voss and Finlay, 2002) by varying the turbulence levels and pattern of particle–particle and particle–device collisions. However, few previous experimental studies have addressed the physical mechanism of DPI operation, and it remains poorly understood. At a fundamental level this is the fluidisation of an initially stationary powder bed (a single patient dose) into the inhaled airstream. The work of Wang et al. (2004) and Versteeg et al. (2005) has begun to address this research area for impinging jet inhaler designs (where the bed of powder is aerosolised by a vertical jet of air). Wang et al. (2004) quantifies the effect of various inhaler design changes by measuring the FPF output of an idealised DPI. However, this work still does not address the question of how the fluidisation process occurs within the inhaler. Versteeg et al. (2005) use an optical technique to record high speed video of the fluidisation process. They repeat this for a number of different lactose powder grades and dose reservoir geometries for an impinging jet fluidisation. The study concludes that the initial mechanism of powder bed break-up is by shear fluidisation, with the particles entrained into the flow layer-by-layer, producing a slow particle source. Following this process, the jet flow penetrates the powder bed and aerates the entire bed from the centre, producing a fast particle source. These qualitative results are useful, but little quantitative data is extracted, and few differences are observed over the range of dose reservoir geometries, applied inhalation pressure profiles or powder types tested.

The aim of this study is twofold. Firstly to experimentally examine the dose fluidisation within a DPI to identify different types of behaviour, and secondly to assess whether this field also experiences the problem of inadequate powder material property characterisation using traditional bulk methods. A similar optical technique to Versteeg et al. (2005) was used to record high speed video of the powder dose fluidisation from various 'inline' (rather than impinging jet) idealised DPI geometries. In addition to studying a different type of inhaler design, a wider range of powder types were tested, with distinct contrasts being observed in the fluidisation of different powders. As well as qualitative observations of the fluidisation, a quantitative measure of the extent of the dose fluidisation over time was evaluated. This is presented to directly compare dose fluidisations under different conditions. Bulk powder properties are quantified using an annular shear tester to assess whether such measurements can be used to predict the mechanism of fluidisation within a DPI.

2. Materials and methods

2.1. Materials

Four different powder types were tested: spherical glass particles sized 0–50 μm (Jencons), aluminium particle flakes in the range 0–44μm ('−325 mesh', VWR), lactose '6.0% fines' , and lactose '16% fines'. The 'percentage fines' of the lactose refers to the mass fraction of particles smaller than 15 μm in the powder. Both lactose powders were supplied by GlaxoSmithKline.

2.2. Annular shear testing

The bulk flow properties of each powder were measured using a RST-XS annular ring shear tester controlled by RST-Control 95 software (both from Dietmar Schulze Schüttgutmesstechnik, Wolfenbüttel, Germany). The powders were stored at 25 ± 1 °C and 44% relative humidity (RH) for 48 h prior to the analysis, which was carried out in an air conditioned laboratory maintained at 25 ± 1 °C and 35 ± 3% RH. For each test, a 30 mL annular shear cell was filled without applying force to the upper surface of the powder bed. The sample was pre-sheared with a normal stress of 2500 Pa (σ_{pre}) until steady-state flow was achieved. A σ_{pre} value of 2500 Pa was chosen to reflect the consolidation stresses encountered by pharmaceutical powders during small scale powder handling and dosing operations (Schulze, 2005). A yield locus was constructed for each powder by measuring the shear stress required to cause the powder to fail under four normal stresses less than σ_{pre} (500, 1000, 1500 and 2000 Pa) and various flow properties were calculated using the instrument software. The averages of these properties over three repeated tests is presented in Table 1.

2.3. Optical DPI dose fluidisation

An experimental rig was built to assess the influence of three factors on DPI operation: patient inhalation, geometry and powder type. The central feature of the rig was a near 1:1 scale dose reservoir chamber machined from optically clear perspex. This reservoir was filled with powder and attached to a pressure regulation device

Table 1
Powder flow properties measured from the annular ring shear testing, alongside particle density and diameter from Stevens et al. (2007)

	Glass	Lactose 6% fines	Aluminium	Lactose 16% fines
Unconfined yield strength, σ_c (Pa)	503	696	1597	2174
Flowability, ff_c	9.43	7.30	3.40	2.45
Cohesion, τ_0 (Pa)	143	174	410	520
Bulk density, ρ_b (kg m^{-3})	1472	785	940	720
Solid density, ρ_s (kg m^{-3})	2500	1550	2700	1550
Porosity, ε	0.41	0.49	0.65	0.52
Mean particle diameter, d_p (μm)	45	80	–	70

that simulated a patient inhalation. High speed digital video was recorded of the reservoir during the inhalation to capture the process of powder fluidisation. The details of inhalation simulation, reservoir geometry, powder types and video recording are outlined in the rest of this section.

A patient inhalation is usually modelled as a constant flow-rate process, with a value of 60 L min^{-1} used as a typical value (United States Pharmacopoeial Convention, 2000). However, this approach introduces an unrealistic step-change in pressure and flow-rate at the start of an inhalation that is not well controlled (Chavan and Dalby, 2002). Such a step-change is not seen in real patient inhalation pressure profiles. Some evidence exists to suggest this step-change does not have a significant effect on the generated exit FPF for some DPIs (Finlay and Gehmlich, 2000), but it will affect the initiation of the dose fluidisation. An alternative approach was used in this study: the inhalation was simulated by regulating the pressure drop applied across the dose reservoir over time. The pressure drop produced by a typical patient increases approximately linearly for the first 0.3 s of the inhalation with a gradient of 30 kPa s^{-1} (Palmer, 2004). Since the fluidisation of the powder in the reservoir occurs in the first 0.2 s of the inhalation, the complete inhalation was modelled as a linearly increasing pressure drop. Significant variation in inhalation strength is seen between different patient groups (Quanjer et al., 1993)(e.g. adults and children, smokers and non-smokers) and a number of different gradients were used to simulate different patient types: 3.3, 10 and 30 kPa s^{-1}. The pressure drop was dynamically regulated by using a pressure sensor at the reservoir outlet to control a solenoid flow control valve attached to a vacuum source (Fig. 1). In this way, the predetermined pressure drop profile across the reservoir was maintained regardless of inhaler geometry or particle type.

Three idealised reservoir geometries were tested, labelled 0 °, 45° and 90° (inset, Fig. 1). The air-flow though each reservoir exerts a different combination of shear and normal forces on the powder dose. A powder dose in the 0° reservoir is subject to primarily shear loading, in the 90° reservoir to mainly normal loading, and in the 45° reservoir both shear and normal forces. The powder volume in both 0 and 90° reservoirs is equal, measuring 6 mm ×2 mm ×2 mm. The 45° reservoir encloses the same volume, but with the inlet and exit edges inclined at 45°. A channel of 2 mm ×2 mm square cross-section enters and exits all reservoirs: the inlet channel is open to the atmosphere and the outlet channel is connected to the inhalation pressure regulator. The inlet channel is long enough to ensure fully developed flow at the reservoir entry (a minimum length of 140 mm). The reservoirs can be disassembled to refill the powder chamber—a spatula is used to overfill the reservoir then the excess skimmed to level the powder fill. The powder is not otherwise compacted, and initial work confirmed that the skim direction had no effect on the results obtained. Although the reservoir filling process is not automated, the same tester always filled the reservoir and as the test matrix encompassed over 500 individual tests, reservoir refilling became an accustomed and consistent process by that tester.

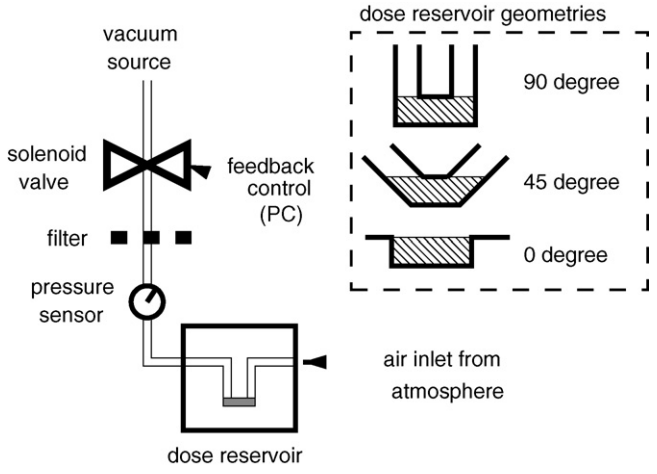

Fig. 1. A schematic (not to scale) of the pressure regulation system. The three dose reservoir geometries are illustrated (inset), with hatching representing the powder fill volume.

A digital Kodak MX4540 camera (on loan from the EPSRC) was used to record video of the dose reservoir during the simulated inhalation. The camera recorded a series of 256 × 256 pixel images at a frequency of 4500 frames per second (FPS). During recording, the powder in the reservoir was back-lit using twin 1 kW halogen lamps. Although it was not possible to regulate the local ambient temperature, pressure and humidity conditions during this testing, the temperature fluctuations produced by the halogen lighting were reduced to a minimum by illuminating the reservoirs only when necessary. Each fluidisation test was repeated three times. Some tests were performed a further three times after a week period, with the entire experimental rig disassembled, cleaned with high pressure air, and reassembled in this interval. These results are compared in Section 3.3 to assess the repeatability of the results.

3. Results and discussion

In a DPI the airstream passes through the powder dose, fluidising portions of the initially stationary bed into the flow. This flow carries the fluidised particles out into the lungs of the patient. The ability of the airflow to fluidise (i.e. separate) particles depends both on the flow properties of the powder and the energy contained within the flow. By evaluating the bulk powder flow properties (shear test results in Section 3.1) separately from the combined effect of powder properties and airflow (qualitative and quantitative optical DPI results in Sections 3.2 and 3.3), this study assesses whether this bulk method of particle characterisation can be used to predict powder behaviour within a DPI.

3.1. Powder characterisation

Bulk powder flow properties were quantified by annular shear testing, and various relevant measured properties are presented in Table 1. Particle shape affects these properties, and typical shapes of

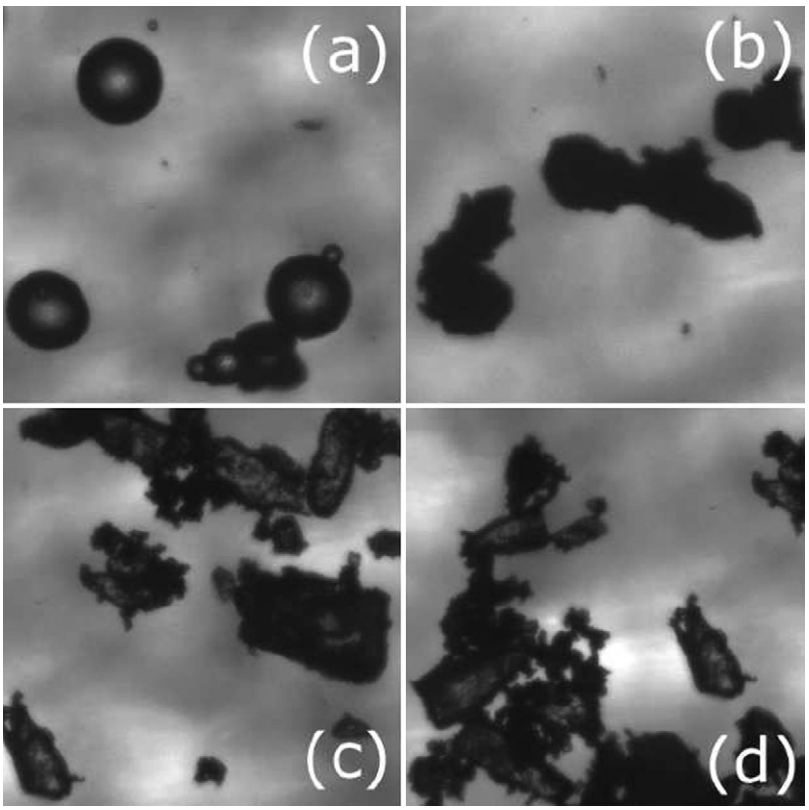

Fig. 2. Light micrograph images of the four different powder types: (a) glass spheres, (b) aluminium flakes, (c) lactose 6% fines and (d) lactose 16% fines.

each powder tested are illustrated by the light micrograph images in Fig. 2.

The bulk density, ρ_b, should be distinguished from solid density, ρ_s: solid density is that of individual particles, whereas bulk density is that of an entire powder bed (including any void space). The bulk density depends strongly on the powder bed consolidation stress (i.e. the bed 'compaction'). The porosity (ε) is the ratio of the volume of all voids in a powder bed to the total volume, and is calculated from the measured bulk and solid density. The porosity provides a measure of the ease with which a flow can move through a stationary bed of powder—the higher the porosity, the more void space is available for the air to flow through.

The unconfined yield strength, σ_c, is the normal stress required to break or fracture a consolidated powder bed. The flowability of the bulk powder is numerically characterised by the steady state flowability ratio, ff_c, of consolidation stress to unconfined yield strength. The larger this ratio, the better the bulk powder flows. The tested powders in order of decreasing steady state flowability are glass, lactose 6% fines, aluminium, lactose 16% fines. Note that the bulk flowability ratio, in common with all the properties measured by the shear test, is a measured under steady state conditions. In contrast, the process of fluidisation that occurs within the DPI is inherently a transient one, and care must be taken attempting to draw parallels between them.

The ability of particles to separate from one another depends on the particle–particle bonding or cohesion. Highly cohesive powders may not fluidise easily, and can form large agglomerates of many individual particles. Shear testing measures bulk particle cohesion, τ_0, as the shear stress required to break or fracture a consolidated powder bed with zero normal stress. Although this value gives an indication of the steady state *bulk* cohesivity, it is not clearly related to the transient fundamental particle–particle bonding forces (Jones, 2003).

The powders tested in this study are all members of Geldart's group A as illustrated by Fig. 3. Mean particle diameter data for both glass and lactose powders has been taken from a previous study (Stevens et al., 2007), and is included in Table 1. Although no such data exists for the aluminium particles, the sieved diameter range is 0–44 μm and it is speculated that the mean diameter will be in the range from 30 to 44 μm.

3.2. Qualitative analysis

We observed two distinct methods of powder bed break-up: a 'fracture' and an 'erosion' mechanism. Under the erosion mechanism the particles do not form any large agglomerates, and are

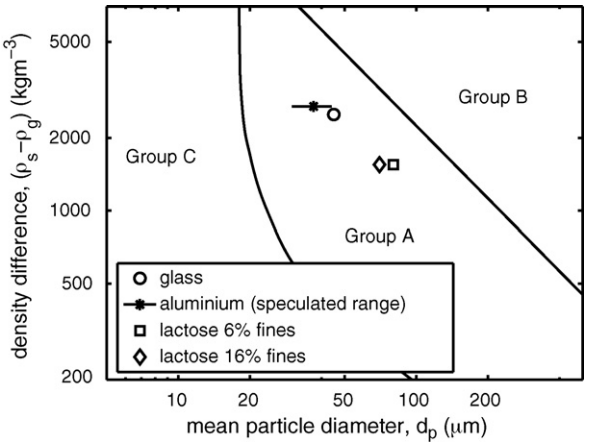

Fig. 3. A logarithmic plot of the empirical Geldart powder group boundaries. The position of the glass, lactose 6% fines, lactose 16% fines are plotted along with the speculated position of the aluminium powder.

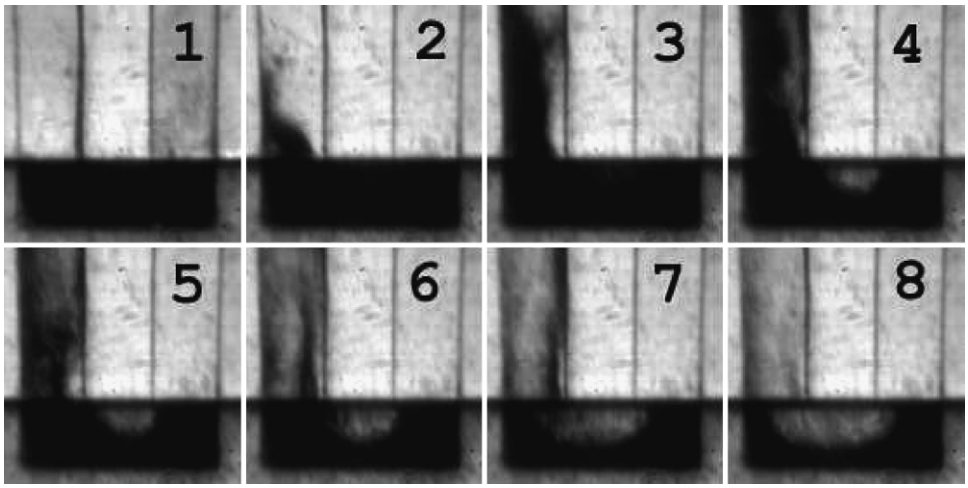

Fig. 4. A sequence of frames illustrating the fluidisation of glass powder from the 90° dose reservoir under the influence of a 30 kPa s^{-1} pressure drop gradient. The right hand leg is the entry and the left hand leg has the low pressure applied, inducing flow into that leg. The initial frame is taken 0.022 s into the inhalation, and subsequent frames are included after every 0.011 s.

entrained into the airflow as individual particles or small agglomerates. For the 90° and 45° reservoir geometries (where the powder bed blocks the airflow at the start of an inhalation) the flow creates a small channel through the bed at the apex of the U-bend. This channel gradually enlarges as the flow picks up particles from the surrounding powder. This process continues until the reservoir is empty.

Fig. 4 shows a sequence of video frames that illustrate a typical erosion dose fluidisation. Note that since the reservoir is back-lit, the powder is visible as darker areas, and the inhalation airflow direction is from right to left through the U-shaped geometry. The observed erosion fluidisations were very consistent within repeated tests: Fig. 5 shows a single frame at identical times from six repeated tests of an erosion glass powder fluidisation. The tests were performed in two consecutive batches of 3 (arranged on the figure in two rows), separated by a week period in which the optical DPI was entirely dismantled and then reassembled.

Under a 'fracture' mechanism the packed powder bed separates along lines of weakness, and these 'cracks' often form across the entire height of the reservoir. This results in the entrainment of large agglomerates into the main flow (pieces of the packed bed that have been separated by these cracks). The complete fluidisation of the dose typically occurs faster than under an erosion mechanism, and large particle agglomerates can be clearly observed in the reservoir outlet channel. Fig. 6 shows a typical fracture fluidisation as a sequence of video frames. In contrast to the erosion mechanism, although repeated tests displayed the same pattern of fluidisation, in each case the powder bed fractured in an irregular fashion which was impossible to predict. Fig. 7 shows a single frame from six repeated tests of a lactose 16% fines fluidisation. Again, these tests were performed in two batches of three separated by a week period.

This fracture fluidisation behaviour is typical of Geldart group C powders (Wang et al., 1998). Such powders are difficult to fluidise and tend to form large agglomerates and powder 'slugs' as the fluid

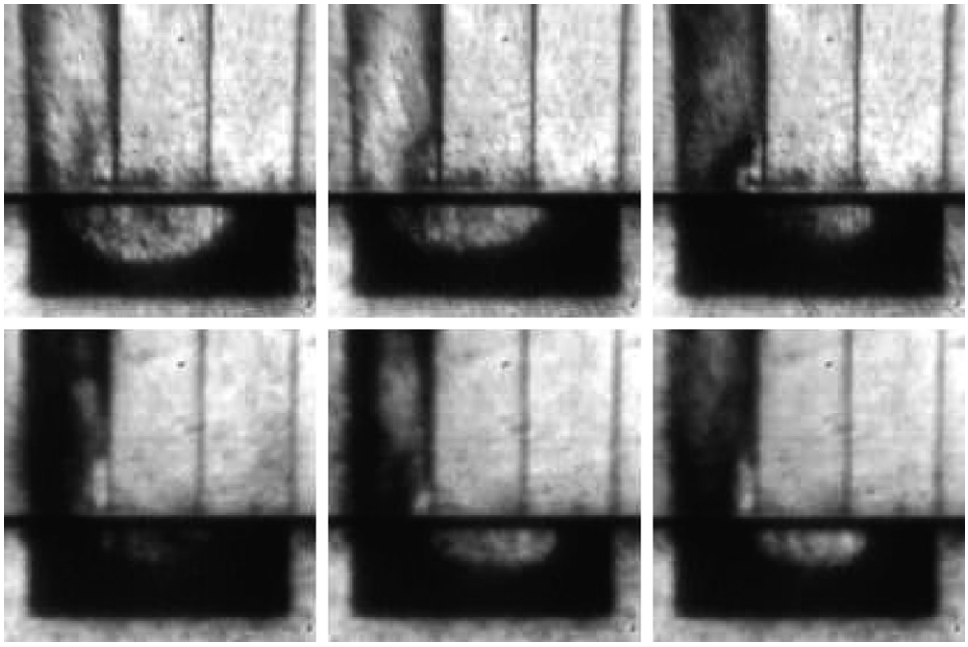

Fig. 5. A single frame from six different glass particle fluidisation tests with a 30 kPa s^{-1} pressure drop gradient. All frames were captured at an identical time of 0.08 s.

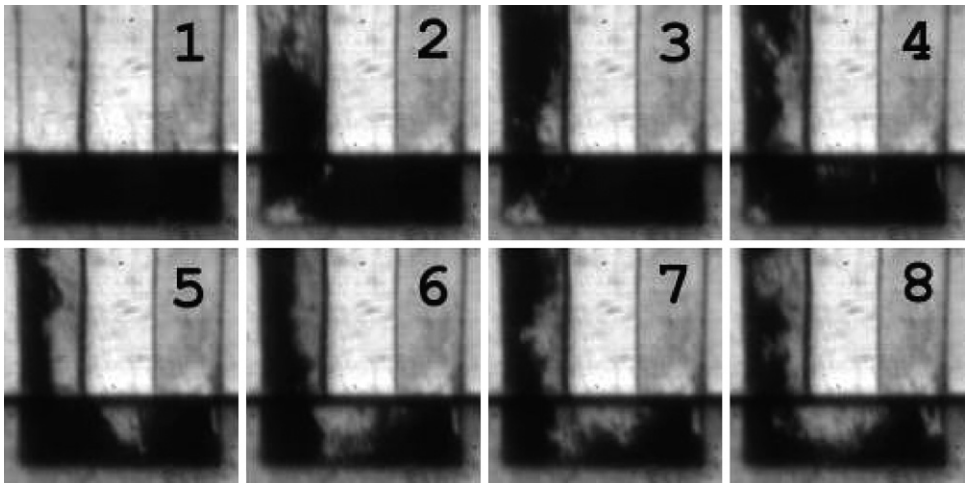

Fig. 6. A sequence of frames depicting the fluidisation of lactose 16% fines powder from the 90° dose reservoir under the influence of a 30 kPa s^{-1} pressure drop gradient. The initial frame is taken 0.033 s into the inhalation, and subsequent frames are included after every 0.003 s.

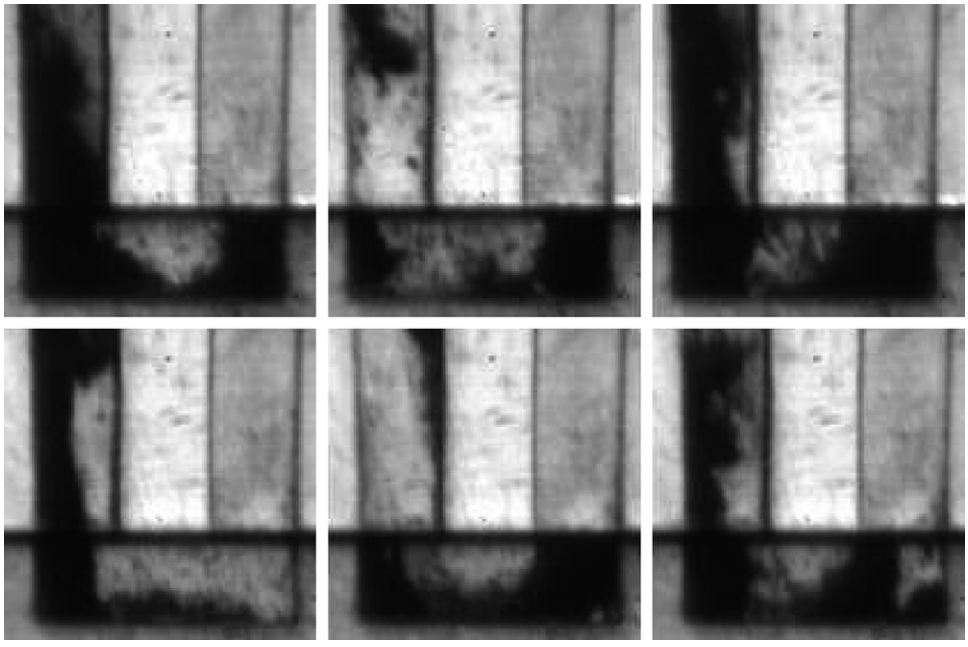

Fig. 7. A single frame from six different lactose 16% fines particle fluidisation tests with a 30 kPa s^{-1} pressure drop gradient. All frames were captured at an identical time of 0.05 s.

pressure builds up until the whole powder bed moves at once. Fig. 8 shows a close-up (in the centre of a 90° reservoir) of the formation of such a powder slug that spans the entire reservoir height.

The mechanism of dose fluidisation was observed to be consistent for each powder tested whatever the reservoir geometry or applied pressure drop gradient. Glass and aluminium powder fluidisations were visually indistinguishable, occurring with an erosion mechanism. The fluidisation of lactose 16% fines occurred under a fracture mechanism. The lactose 6% fines powder exhibits a milder fracture mechanism than the 16% fines powder: cracks still

Fig. 8. A sequence of frames from the fluidisation of lactose 16% powder showing a full channel-width powder bed fracture. The area shown in the 4 frames (at times 0.049, 0.050, 0.051 and 0.052s) is the centre of the reservoir, highlighted in the full reservoir image on the left. The images have been converted to binary black and white to improve clarity.

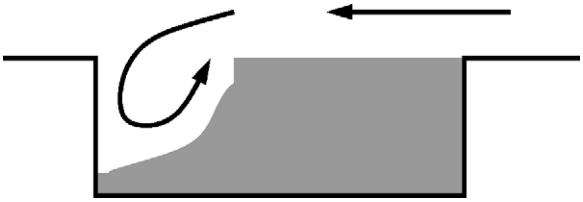

Fig. 9. A diagram illustrating the typical flow in the 0° dose reservoir. Note the recirculation zone at the trailing edge of the reservoir that lifts the powder up into the main airflow.

form in the powder bed and large agglomerates were entrained into the airflow, but the agglomerate size was typically smaller than those observed in the fluidisation of the 16% fines powder.

The rate of fluidisation increased with a larger pressure drop gradient (i.e. stronger inhalation) for all powders and reservoir geometries tested. This effect is discussed further in the presentation of the quantitative results (Section 3.3). Other than a change in the fluidisation rate, no other differences induced by varying the applied pressure drop gradient were observed. For example, the mechanism of fluidisation remained independent of the applied pressure drop gradient for the range tested.

The reservoir geometry had a significant effect on the dose fluidisation process, although the bed break-up mechanism (erosion or fracture) remains consistent for each powder type. Fluidisation in the 90° and 45° reservoirs have similar traits: in both cases the powder dose initially blocks the airflow and the visually observable differences in powder fluidisation are minimal. Fluidisation from the 45° reservoir occurs at a slightly lower pressure drop across the reservoir and in a shorter time than the 90° reservoir. In addition, there are less fluid flow artifacts (such as the small recirculation zone that forms at the square corners of the 90° reservoir).

The powder bed in the 0° reservoir does not block the airflow, and this prompts a different dose fluidisation process to that seen in either the 90° or 45° reservoirs. Although the overall process is different, the bed break-up mechanism (erosion or fracture) remains consistent with the other geometries for each particle type. A recirculation zone forms at the downstream edge of the 0° reservoir and pushes the particles up into the main channel where they are entrained into the flow out of the reservoir. Fig. 9 shows a schematic of the process, and Fig. 10 contains a sequence of images illustrating the process for both glass and lactose 16% fines powder.

3.3. Quantitative analysis

The fluidisation videos from the 90° reservoir were post-processed to quantitatively compare the effect of different powder types and pressure drop gradients. We used the mean pixel intensity of the reservoir as a measure of the amount of powder in this area. The intensity was measured as a normalised value between 0 and 1. Black has an intensity of 0, and pure white an intensity of

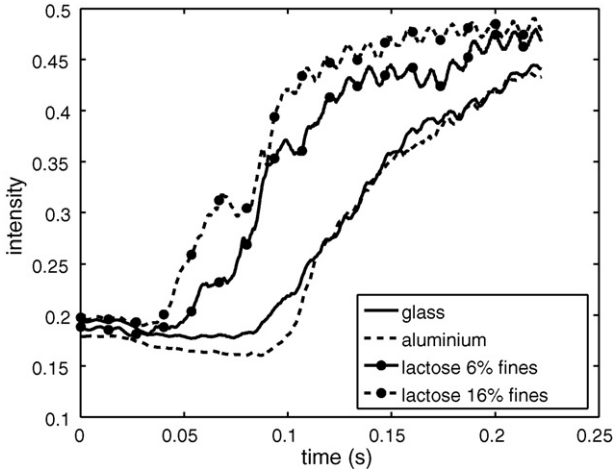

Fig. 11. 90° reservoir intensity plotted against time under the influence of a -30kPa s^{-1} pressure drop gradient. Note that each plotted fluidisation (i.e. a single data line) is the mean average of three repeated tests.

1. At the beginning of a test the reservoir is completely filled with powder and little light passes through to the camera which results in a low mean intensity (typically 0.2). As the powder is entrained into the airflow and leaves the reservoir, there is less powder to block the passage of the back-lighting to the camera, and the intensity increases. It reaches a maximum value of about 0.5 when the reservoir is completely emptied. The intensity over the duration of a test can be plotted against either the pressure drop across the reservoir or the time to quantitatively characterise a fluidisation.

Fig. 11 illustrates the 90° reservoir intensity plotted against time under the influence of a -30 kPa s^{-1} pressure drop gradient. The figure confirms that the fluidisation of lactose 16 and 6% fines occurred at a faster rate than either aluminium or glass. The glass and aluminium powder fluidised via a gradual erosion mechanism, whilst the lactose blends fluidised through fracture. The plot shows that the fracture process produces a quicker emptying of the reservoir than an erosion mechanism under the same applied pressure drop gradient. Although the figure illustrates data from just one pressure drop gradient, similar patterns held true for the other gradients tested. Fig. 12 plots the same intensity data against the pressure drop across the reservoir instead of time. It shows that the lactose powders fluidise at a lower pressure difference across the powder bed than either aluminium or glass. In addition, both Figs. 11 and 12 show that aluminium and glass have very similar fluidisation patterns. This confirms the qualitative observation that the fluidisation of the two powders was visually indistinguishable.

Note that each fluidisation line plotted in these diagrams is the mean of three repeated tests performed consecutively. This produces consistent results and smoothes out any test-to-test variation in the fracture mechanism fluidisations. For example, Fig. 13 illus-

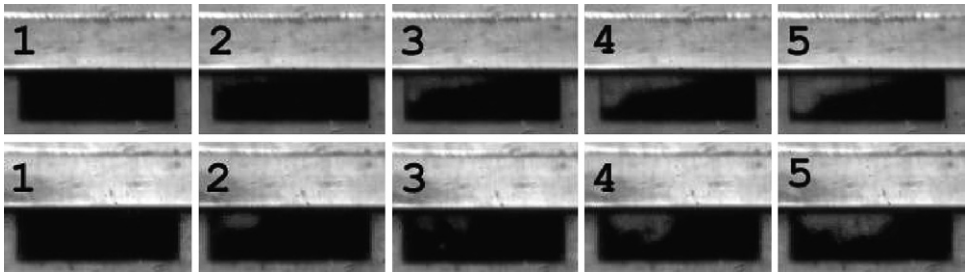

Fig. 10. Two video frame sequences depicting the fluidisation of lactose 16% fines (bottom) and glass powder (top) from the 0° reservoir with a pressure drop gradient of -30 kPa s^{-1}. The initial frame is taken after 0.26s for glass, and 0.18s for the lactose 16% fines. Subsequent frames for both powders are shown at 0.06 s intervals.

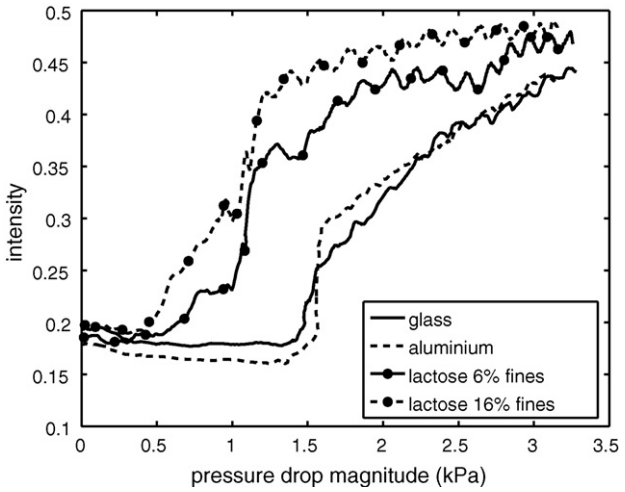

Fig. 12. This plot illustrates the same data as Fig. 11, but plots the intensity against the pressure drop across the reservoir instead of time.

trates two batches of lactose 16% fines data plotted on the same diagram. Each 'batch' consisted of three tests performed consecutively, and the two sets were separated by a week period in which the optical DPI was dismantled and reassembled.

Figs. 14 and 15 show the 90° reservoir intensity data for lactose 16% fines powder under a number of different pressure drop gradients. Fig. 14 shows that a larger pressure gradient produces a proportionally faster fluidisation. Fig. 15 shows that for all gradients, the extent of the reservoir emptying process is dependent only on the pressure, and is independent of the pressure gradient. It is speculated that this independence can be attributed to the fracture mechanism of fluidisation that lactose 16% fines undergoes. As the pressure increases, the force exerted on the powder bed increases, and parts of the bed will fracture and become entrained in the flow when this force reaches a critical value. The rate at which this force changes, or the time taken to reach the critical force does not affect the powder bed. We observed a similar pattern for the lactose 6% fines powder, but glass and aluminium powders appear to exhibit quite different behaviour.

Fig. 16 shows intensity data for the glass powder. In this case, the amount of powder remaining in the reservoir at a particular

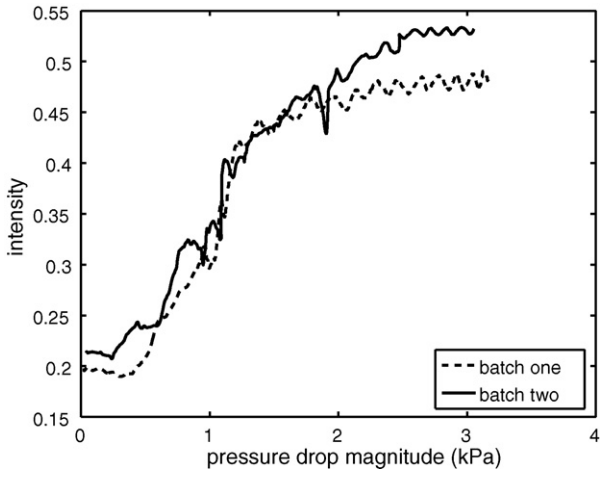

Fig. 13. 90° reservoir intensity plotted against pressure under the influence of a $-30\,\mathrm{kPa\,s^{-1}}$ pressure drop gradient for lactose 16% powder. Data from two different batches of repeated tests are plotted. These test batches were separated by a week period in which the optical DPI was dismantled and reassembled.

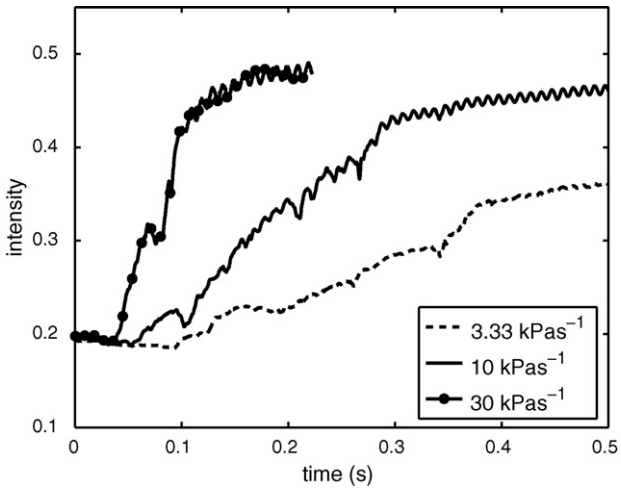

Fig. 14. 90° reservoir intensity plotted against time for lactose 16% fines powder.

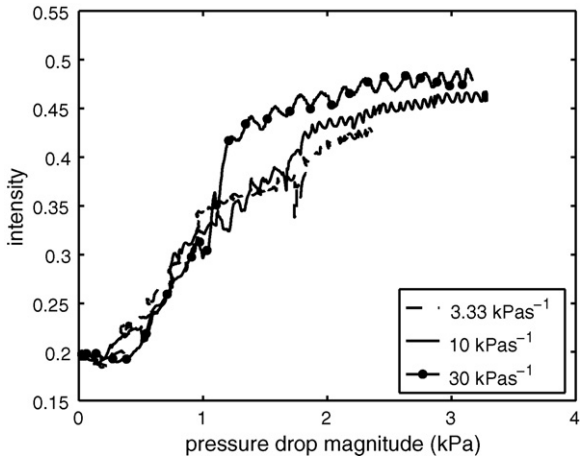

Fig. 15. 90° reservoir intensity plotted against pressure drop for lactose 16% fines powder.

pressure *is* dependent on the pressure drop gradient. The intensity data for the aluminium powder exhibits a similar pattern. There are a number of possible explanations for this observed effect. The number of particles entrained may be dependent on the length of time that the powder bed has been exposed to the flow. New

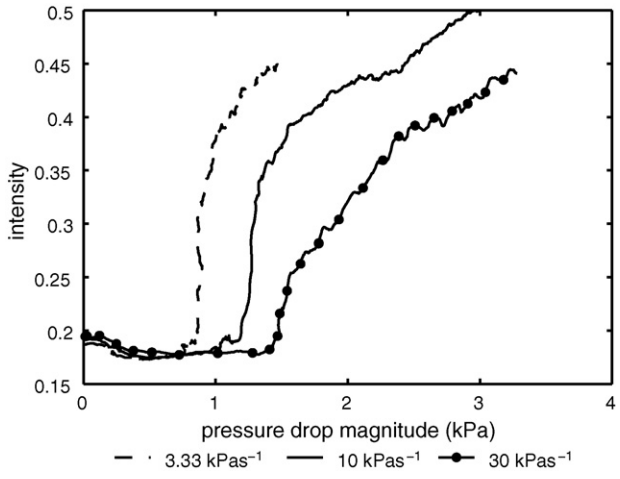

Fig. 16. 90° reservoir intensity plotted against pressure drop for the glass powder.

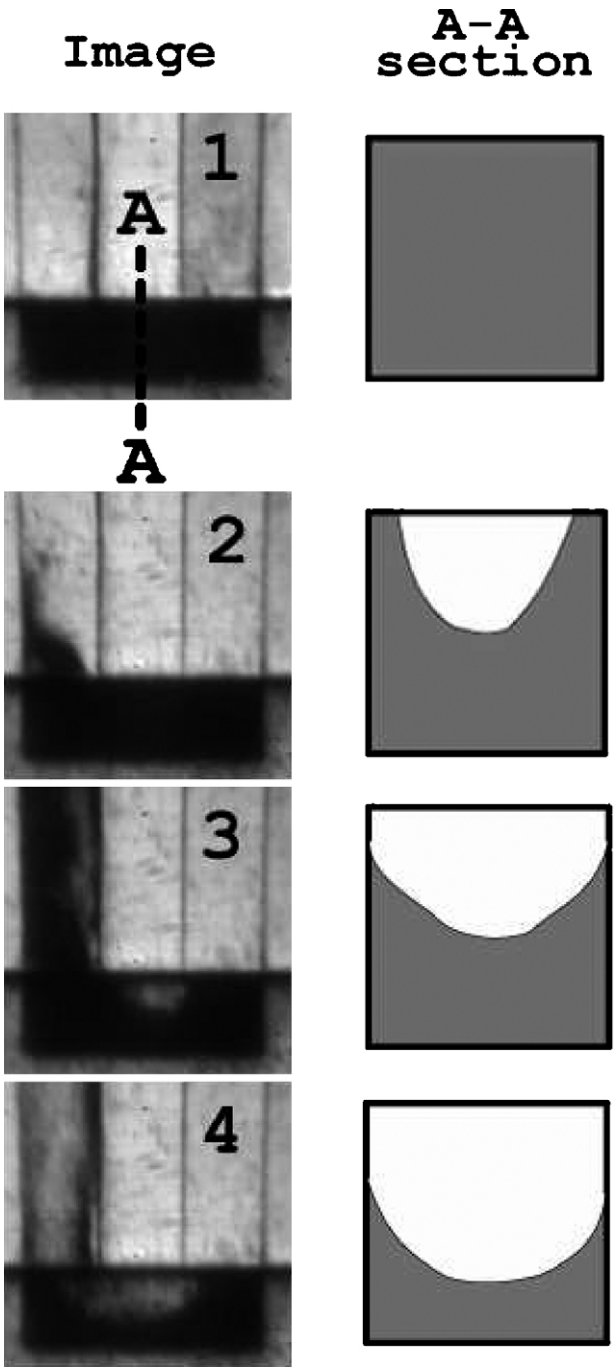

Fig. 17. Speculated reservoir cross-sections under an erosion fluidisation, alongside the observed 2D images. Note frame 2 in particular—although there is airflow passing through the reservoir (and powder entrained into the outlet flow), the powder at the side of the reservoir obscures the 2D view of the channel.

particles are entrained only once the layer of particles on top of them have been removed, and this layer-by-layer stripping of the bed is likely to be time dependent. Alternatively, it should be noted that the experiment we conducted measures a three-dimensional (3D) process with a 2D methodology: by using back-lighting to view the reservoir, any variation across the width of the reservoir is obscured. For example, the speculated 3D process of an erosion fluidisation is illustrated in Fig. 17 alongside the 2D images recorded. This 2D approximation may introduce inaccuracies in the presented quantitative results.

3.4. Characterising the fluidisation method

The experimental results presented and discussed in Sections 3.2 and 3.3 clearly demonstrate two distinctly different powder bed break-up mechanisms in the dose reservoir, erosion and fracture. In our results the mechanism depended solely on the powder type, and remained consistent for all reservoir geometries and pressure drop gradients. This is similar to both fluidised bed technology and pneumatic conveyance, in that the powder properties are the dominate factor in determining the system behaviour. Thus it should be possible to predict the mechanism that occurs within a DPI for any powder based on its material properties. The tested powders can be grouped by break-up mechanism (lactose 16 and 6% fines fracture, glass and aluminium particles erode), to search for a matching pattern in their bulk properties (Table 1).

Ranking the tested powders by the bulk parameters measured by a shear tester (e.g. flowability, unconfined yield strength, cohesion, porosity) produces the list: glass, lactose 6% fines, aluminium and then lactose 16% fines. Clearly none of these bulk parameters provide a possible indication of the fluidisation mechanism. However, the same grouping as that by mechanism occurs in the Geldart classification (Fig. 3), based on the solid density and average particle size. Indeed, we speculate that the lactose blends have been misclassified in this instance and behave as group C powders. This may be due to the insensitivity of the Geldart classification to the proportion of fines within a lactose blend, as it is based on a volumetrically averaged particle diameter. However, the limited number of powders tested make the formation of any mechanism prediction rules impossible at present, and further work is required in this area.

4. Conclusion

We have identified two distinct mechanisms of dose fluidisation from inline DPIs, labelled ‘erosion’ and ‘fracture’ in this paper. Similar to fluidised beds and pneumatic conveyance, the dominate factor determining this mechanism is the powder material properties. In the range tested the mechanism is independent of dose reservoir geometry or pressure drop gradient (i.e. inhalation type). Of the powders tested, both lactose powders (6 and 16% fines) exhibited a fracture fluidisation, and aluminium and glass fluidised through an erosion mechanism.

The fracture mechanism results in large agglomerates breaking off from the powder bed as it cracks along lines of weakness. The alternative erosion mechanism is slower: a small channel forms through the powder bed which gradually enlarges until all the powder is entrained into the inhalation flow. The fracture mechanism occurs faster and initiates at a lower pressure drop across the dose reservoir than the erosion mechanism for the powders tested.

Quantitative analysis of the lactose fracture mechanism has shown that the fraction of the DPI dose fluidised depends on the instantaneous inhalation pressure only, and is independent of the pressure profile history. This is not true for the erosion mechanism of aluminium or glass powder, which exhibits a dependence on the previous pressure profile history of the inhalation.

In common with fluidised bed technology and pneumatic conveying behaviour, the mechanism of dose fluidisation cannot be predicted using bulk powder properties (such as flowability or unconfined yield stress measured by a shear tester). Although some similarity exists with the fluidised bed Geldart powder classification, further work is required in this area before any conclusions extending beyond the currently examined powders can be reached.

Acknowledgements

This work was undertaken with the financial support of the EPSRC and GlaxoSmithKline.

References

Borgstrom, L., Bisgaard, H., O'Callaghan, C., Pedersen, S., 2002. Dry powder inhalers. In: Bisgaard, H., O'Callaghan, C., Smaldone, G. (Eds.), Drug Delivery to the Lung. Marcel Dekker Inc., pp. 421–448.

Chan, H., 2006. Dry powder aerosol delivery systems: current and future research directions. J. Aerosol Med. 19, 21–27.

Chavan, V., Dalby, R., 2002. Novel system to investigate the effects of inhaled volume and rates of rise in simulated inspiratory air flow on fine particle output from a dry powder inhaler. AAPS PharmSci 4, 1–6.

Chew, N., Chan, H., 2002. The role of particle properties in pharmaceutical powder inhalation formulations. J. Aerosol Med. 15, 325–330.

Clark, A., Borgstrom, L., 2002. In vitro testing of pharmaceutical aerosols and predicting lung deposition from in vitro measurements. In: Bisgaard, H., O'Callaghan, C., Smaldone, G. (Eds.), Drug Delivery to the Lung. Marcel Dekker Inc., pp. 105–142.

Dixon, G., January 1979. The impact of powder properties on dense phase flow. International Conference on Pneumatic Conveying, London, UK, pp. 1–14.

Dunbar, C., Hickey, A., 2000. Evaluation of probability density functions to approximate particle size distributions of representative pharmaceutical aerosols. J. Aerosol Sci. 31, 813–831.

Finlay, W., Gehmlich, M., 2000. Inertial sizing of aerosol inhaled from two dry powder inhalers with realistic breath patterns versus constant flow rates. Int. J. Pharm. 210, 83–95.

Geldart, D., 1973. Types of gas fluidisation. Powder Technol. 7, 285–292.

Jones, R., 2003. From single particle afm studies of adhesion and friction to bulk flow: forging the links. Granul. Matter 4, 191–204.

Molerus, O., 1996. Overview: pneumatic transport of solids. Powder Technol. 88, 309–321.

Newman, S., Pitcairn, G., December 2005. New horizons in drug delivery imaging. In: Drug Delivery to the Lungs, vol. 16. The Aerosol society, pp. 27–32.

Palmer, M., 2004. Inhalation pressure profile data from gsk. Personal communication.

Quanjer, P.H., Tammeling, G.J., Cotes, J.E., Pedersen, O.F., Peslin, R., Yernault, J.C., 1993. Lung-volumes and forced ventilatory flows – report working party standardization of lung-function tests european-community for steel and coal – official statement of the european respiratory society. Eur. Respir. J. 6, 5–40.

Sanchez, L., Vasquez, N., Klinzing, G.E., Dhodapkar, S., 2003. Characterization of bulk solids to assess dense phase pneumatic conveying. Powder Technol. 138, 93–117.

Schulze, D., 2005. Flow properties testing with ring shear testers RST-01.01, RST-01-PC and RST-XS, 1st edition.

Shoyele, S., Slowey, A., 2006. Prospects of formulating proteins/peptides as aerosols for pulmonary drug delivery. Int. J. Pharm. 314, 1–8.

Stevens, N., Shrimpton, J., Palmer, M., Prime, D., Johal, B., 2007. Accuracy assessments for laser diffraction measurements of pharmaceutical lactose. Meas. Sci. Technol. 18, 3697–3706.

Sundaresan, S., 2003. Instabilities in fluidized beds. Annu. Rev. Fluid Mech. 35, 63–88.

United States Pharmacopoeial Convention, 2000. Physical tests and determinations, section 601: aerosols. In: United States Pharmacopeia. National Publishing, pp. 1895–1912.

Versteeg, H., Hargreave, G., Hind, R., December 2005. An optical study of aerosol generation in dry powder inhalers. In: Drug Delivery to the Lungs, vol. 16. The Aerosol society, pp. 3–6.

Voss, A., Finlay, W., 2002. Deagglomeration of dry powder pharmaceutical aerosols. Int. J. Pharm. 248, 39–50.

Wang, Z., Kwauk, M., Li, H., 1998. Fluidization of fine particles. Chem. Eng. Sci. 53, 377–395.

Wang, Z., Lange, C., Finlay, W., 2004. Use of an impinging jet for dispersion of dry powder inhalation aerosols. Int. J. Pharm. 275, 123–131.